Eur. Phys. J. D **10**, 247–257 (2000)

**THE EUROPEAN PHYSICAL JOURNAL D**

EDP Sciences
© Società Italiana di Fisica
Springer-Verlag 2000

# Improved molecular constants for the $X^1\Sigma^+$ and $A^1\Sigma^+$ states of NaH

F.P. Pesl, S. Lutz, and K. Bergmann[a]

Fachbereich Physik, Universität Kaiserslautern, 67663 Kaiserslautern, Germany

Received 21 August 1999

**Abstract.** Improved molecular constants for the $X^1\Sigma^+$ and $A^1\Sigma^+$ states of the NaH molecule are presented. NaH molecules are produced by reactive scattering of H and $Na_2$ in a crossed beam experiment. High vibrational levels ($6 \leq v'' \leq 9$) of the NaH molecules are predominantly populated. Their excitation spectrum in the range 630 nm $\leq \lambda \leq$ 670 nm has been measured using a new variant of Doppler spectroscopy. The transition frequencies involving the vibrational levels $2 \leq v' \leq 8$ in the $A^1\Sigma^+$ and $6 \leq v'' \leq 9$ in the $X^1\Sigma^+$ state have been determined with an accuracy of better than 0.01 cm$^{-1}$. Using also previously published data a new set of molecular constants for the $X^1\Sigma^+$ and $A^1\Sigma^+$ state is derived. In particular, the vibrational dependence of the rotational constants $B, D$ and $H$ as well as some of $v''$–$v'$ band origins for $0 \leq v'' \leq 9$ and $0 \leq v' \leq 25$ is determined. The transition frequencies measured here or published previously are reproduced by these new coefficients with an accuracy of $\leq 0.1$ cm$^{-1}$ [rms value] with a maximum deviation of 0.4 cm$^{-1}$. New RKR potential energy curves have been calculated up to the turning points of the levels $v'' = 9$ in the $X^1\Sigma^+$ state and $v' = 25$ in the $A^1\Sigma^+$ state.

**PACS.** 33.15.Mt Rotation, vibration, and vibration-rotation constants – 33.20.Kf Visible spectra

## 1 Introduction

Spectroscopic investigations of the alkali hydrides in the gas phase have played an important role in the development of molecular spectroscopy and for the analysis of molecular structure. In fact, the NaH molecule was referred to by Dunham [1] himself as a test for his approach to the analysis of the spectra of diatomic molecules. One reason for the particular interest in the alkali hydrides lies in the avoided crossing between the $X^1\Sigma^+$ and the $A^1\Sigma^+$ state due to a strong interaction between the ionic and covalent branches of the potential curves. The $A$-state is flat-bottomed and highly anharmonic. This results in a negative anharmonicity constant $\omega_e x_e$ as well as in an anomalous variation of the vibrational level spacings $\Delta G(v')$ and the rotational constants with the vibrational quantum number $v'$. For low lying vibrational levels the rotational constants $B_{v'}$ and $D_{v'}$ initially increase with $v'$ before they decrease in the usual manner. For high vibrational levels also the shape of the $X^1\Sigma^+$ state potential curve is affected by the avoided crossing. Therefore, NaH and other alkali hydrides have been studied by experimentalists and theorists for many decades [2–23].

One example of important classical spectroscopy on NaH is the work of Hori [2,3], who observed and analysed $X^1\Sigma^+$–$A^1\Sigma^+$ bands in absorption and emission. An adjustment of the vibrational assignment in the $A^1\Sigma^+$ state was reported by Olsson [4], who analysed the isotopic shift between levels of NaH and NaD. The data obtained by Hori and Olsson from absorption spectroscopy in the spectral region of 358 nm $\leq \lambda \leq$ 445 nm cover vibrational levels in the range $0 \leq v'' \leq 3$ and $1 \leq v' \leq 20$. Pankhurst [5] extended the data by adding results from dispersed fluorescence measurements in the range of 460 nm $\leq \lambda \leq$ 645 nm including the vibrational levels $0 \leq v'' \leq 8$ and $1 \leq v' \leq 7$. Experimental data involving $v' = 0$ in the spectral region of 600 nm $\leq \lambda \leq$ 700 nm was first reported by Orth *et al.* [6].

Accurate information about the $X^1\Sigma^+$ state of NaH resulted from the rovibrational spectra obtained by Sastry *et al.* [7] and Maki *et al.* [8] based on conventional spectroscopic methods like millimeter range and Fourier spectroscopy, respectively. Precise data for the electronic ground state acquired by infrared and far infrared laser spectroscopy was reported for the first time in the late eighties in [9,10]. The publications on the spectroscopy of NaH in the gas phase before 1990 were reviewed by Stwalley *et al.* [11]. These authors recommended the molecular constants of Maki *et al.* for the $X^1\Sigma^+$ state and those of Orth *et al.* for the $A^1\Sigma^+$ state.

Recently, Lochbrunner *et al.* [12] have used the Degenerate Four Wave Mixing method to observe spectra of NaH in the near UV and in the blue region. These authors noticed that the Dunham coefficients from Stwalley *et al.* [11] did not fit their spectra. Discrepancies between calculated and measured line positions up to 60 cm$^{-1}$ were

[a] e-mail: bergmann@rhrk.uni-kl.de

observed especially for high rotational levels. Such large discrepancies where observed only for vibrational levels, which were not accessible in the previous experiments. They found that the recommended Dunham coefficient $Y_{12}$ correctly describes the vibrational dependence of the constant $D_{v'}$ up to $v' = 7$. Therefore, they determined new molecular constants for the $A^1\Sigma^+$ state based on the vibrational levels $0 \leq v' \leq 25$ by combining their measurements with data from the literature. New Dunham coefficients and a RKR potential curve of the $A^1\Sigma^+$ state were derived by Al-Tuwirqi *et al.* [13], as well. These authors combined the results of Rafi *et al.* [14] for the levels $v' = 14$–$25$ with the data of Orth *et al.* for $v' = 0$, Pankhurst for $v' = 1$–$7$ and Olsson for $v' = 8$–$13$. They covered the same region of vibrational levels in the excited state as Lochbrunner *et al.* In spite of these improvements of the molecular constants for the $A^1\Sigma^+$ state accurate prediction of transition frequencies is restricted to transitions from the lowest vibrational levels of the electronic ground state. Transitions from higher vibrational levels, such as those measured by Orth, deviate up to 40 $cm^{-1}$ from the calculated ones. These facts suggested the need for more accurate experimental data including higher vibrational levels of the electronic ground state.

The present spectroscopic work is a first step in a detailed study of the $Na_2(v'', J'') + H \rightarrow NaH(v, J) + H$ reaction dynamics [24]. The exothermicity of the reaction (1.22 eV) is sufficient to populate vibrational levels up to $v'' = 10$ in the $X^1\Sigma^+$ state of NaH. We present a study of the NaH spectroscopy in the gas phase with a resolution of better than 0.01 $cm^{-1}$ for transitions from vibrational levels $6 \leq v'' \leq 9$ in the electronic ground state.

## 2 Experiment

The essential components of the experimental set-up are shown in (Fig. 1). The NaH molecules are produced in the crossing region of a $Na_2$ molecular beam and a H-atom beam by the reaction $Na_2(v'' = 0, J'') + H \rightarrow NaH(v, J) + Na$. The supersonic sodium beam source with an orifice of 0.5 mm diameter is operated at a temperature of about 650 °C which corresponds to a vapor pressure of about 60 mbar. About 12% of the particles in the beam are dimers [25] with 99% of them found in the vibrational level $v'' = 0$ of the electronic ground state and about 1% in $v'' = 1$. The beam is collimated to 0.9° by two skimmers with a diameter of 2 mm and 1 mm at a distance of 36 mm and 69 mm, respectively, from the nozzle. The vibrational-rotational population distribution as well as the velocity distribution are monitored by laser induced fluorescence at a distance of 700 mm from the nozzle [26]. For $v'' = 0$ the rotational level population distribution corresponds to a rotational temperature of 17 K for $J'' \leq 10$ and 31 K for $J'' > 10$. The maximum population is found in $J'' = 7$. The state $(v'' = 0, J'' = 7)$ carries about 10% of the total $Na_2$ population. The flow velocity is $u_{Na_2} = 1432$ m/s and the width of the velocity distribution is $\alpha_{Na_2} = 257$ m/s (FWHM).

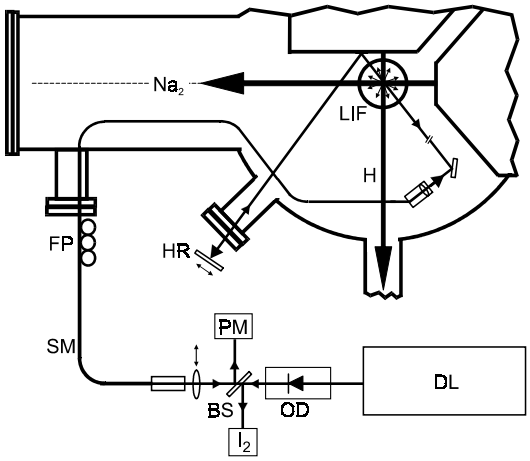


**Fig. 1.** Essential components of the experimental set-up. LIF: high speed detector for laser induced NaH fluorescence; DL: autoscan 699 dye-laser; OD: optical diode; PM: power meter; $I_2$: iodine reference cell; BS: beam splitter (80:20); SM: single mode fibre; FP fibre polarizer; HR: high reflection mirror.

The H-atoms are produced in a 2.45 GHz microwave discharge. The water cooled microwave cavity is placed inside the vacuum apparatus. The pressure in the source is typically 3 mbar and the discharge is normally driven with a microwave power of 40 W. The gas expands through a 0.4 mm orifice into the vacuum and is collimated by a skimmer of 1 mm diameter at a distance of 5 mm from the nozzle, resulting in a collimation of the H-beam of 8.0° (full width). The degree of dissociation is measured with a quadrupole mass spectrometer (QMS) by comparing the signal of mass 2 with the discharge turned on and off. Liquid nitrogen cooling of the quartz walls of the discharge tube is essential in order to dissociate more than 25% of the hydrogen molecules. The velocity distribution which is characterized by a flow velocity of $u_H = 1891$ m/s and a width of the distribution $\alpha_H = 1730$ m/s (FWHM) is determined by time-of flight analysis, using a chopper wheel.

The products are analysed in the reaction zone by laser-induced fluorescence using a single mode dye laser. A single mode fiber (5 $\mu$m core diameter) delivers about 160 mW of power from DCM laser (Coherent 699 Autoscan system, typical linewidth 1 MHz) to the interaction region inside the vacuum chamber. The detector consists of a lens system, which collects 9% of the fluorescence light and images it onto a photomultiplier which is integrated into the detector. Spatial filtering through an aperture of 3 mm diameter serves to suppress background radiation. After collimation the laser beam crosses the reaction region in the scattering plane parallel to the mean relative velocity of $Na_2$ and H, which is at an angle of $\beta = (31 \pm 8)°$ relative to the H-atom beam axis. The laser is subsequently reflected at normal incidence by the mirror HR outside the vacuum. The mirror is adjusted to maximize the fraction of light coupled back into the fiber and observed at the opposite end of the fiber. An optical diode avoids optical feedback to the dye laser.

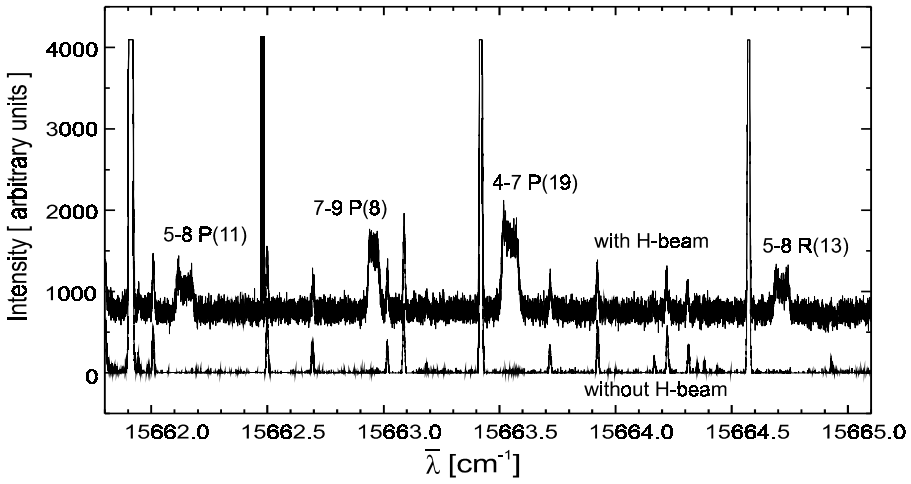


**Fig. 2.** Part of the NaH-spectrum. The NaH-lines are distinguished from the $Na_2$-lines by their linewidth and their lineprofile. The width of the $Na_2$-lines is substantially smaller than that of the NaH-lines. Chopping the H-beam in combination with lock-in detection also allows unambiguous identification of lines related to NaH spectra.

This alignment procedure assures that the incoming and the reflected beam overlap in the region of the reaction center. The laser wavelength was calibrated with an accuracy of 0.001 $cm^{-1}$ using an iodine cell [27].

The excitation spectrum of NaH is measured by laser induced fluorescence (LIF) in the range 620 nm $\leq \lambda \leq$ 670 nm. Since the density of $Na_2$ is about three orders of magnitude larger than the density of NaH and the absorption spectra of these molecules overlap, the emission from $Na_2$ needs to be suppressed by filters. Almost all of the fluorescence light of $Na_2$ is shifted to the red with respect to the excitation wavelength, while a large fraction of the NaH fluorescence is shifted to the blue. Two subsequent shortpass filters with substantial suppression of radiation with $\lambda > 600$ nm were combined to strongly discriminate against the $Na_2$ fluorescence. Nevertheless, the $Na_2$ lines are still observable. Unambiguous identification of spectral features as NaH-lines is based on the line shapes (see Fig. 2) or by chopping the H-atom beam and detecting only the modulated components of the spectrum. Bands of the electronic transition $X^1\Sigma^+$–$A^1\Sigma^+$, including the levels $6 \leq v'' \leq 9$ and $2 \leq v' \leq 8$, are observed with an accuracy of better than 0.01 $cm^{-1}$, using the iodine spectra for calibration. Use of the new NaH *ab initio* potentials of Dern *et al.* [28], which reproduced the data of Orth *et al.*, Maki *et al.* and Lochbrunner *et al.* with a remarkable accuracy of 1 $cm^{-1}$ or better, allowed the unambiguous identification of the observed transitions.

## 3 Analysis of the line profiles

The NaH molecules are formed in a reactive process. The profiles of their absorption lines are therefore determined by the velocity and angular distribution of the products with respect to the direction of propagation of the laser beam. The analysis of these profiles to obtain differential cross-sections for the reactive events will be the subject of another publication [24]. Here, we need only to consider the consequences of the Doppler shift and broadening for the determination of the transition frequencies.

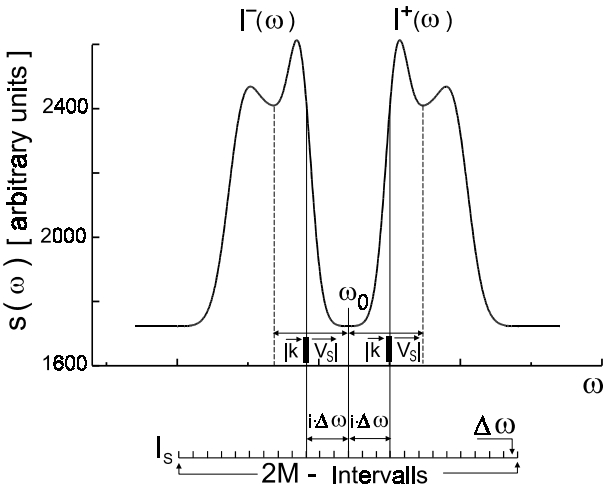


**Fig. 3.** Typical line shape recorded using the back reflection method.

The center frequency $\omega_0$ of a spectral line is Doppler shifted to:

$$\omega(\mathbf{k}) = \omega_0 + \mathbf{k} \cdot \mathbf{V}_s + \mathbf{k} \cdot \mathbf{v}_{cm}^{NaH} \quad (1)$$

where $\omega_0$ is the resonance frequency in the molecular frame, $\mathbf{k}$ is the wave vector of the radiation, $\mathbf{V}_s$ is the velocity of the center of mass and $\mathbf{v}_{cm}^{NaH}$ is the velocity of the product molecule in the center-of-mass system. Upon reflection of the laser beam ($\mathbf{k} \Rightarrow -\mathbf{k}$) a mirror image of the spectrum, induced by the incoming laser, is produced. A spectral component $\omega(\mathbf{k})$ is mapped into one at $\omega(-\mathbf{k})$. The two spectral profiles, $I^+(\omega)$ and $I^-(\omega)$, are symmetric with respect to the resonance frequency $\omega_0$. The centers of gravity of the two spectral lines are separated by $\Delta\omega = 2|\mathbf{k} \cdot \mathbf{V}_s|$ (see Fig. 3), with typical values of 0.05 $cm^{-1} \leq \Delta\omega \leq$ 0.06 $cm^{-1}$. The width of the line profiles ranges from 0.03 $cm^{-1}$ to 0.08 $cm^{-1}$ depending on the kinetic energy of the product molecule, which is related to its internal energy. Details of the line profiles are determined by the reaction dynamics, in particular by the angular distribution of the products.

Now we will discuss the determination of the resonance frequency $\omega_0$ from the spectral lines. The profiles $I^{\pm}(\omega)$ are scaled for equal area before the center of gravity of the two profiles, expected at $\omega_0$, is determined. From the observed spectral profiles of a given transition we calculate

$$\lambda = \frac{\int I^{+}(\omega)\mathrm{d}\omega}{\int I^{-}(\omega)\mathrm{d}\omega} \tag{2}$$

using integration boundaries which do not overlap and scale the intensities according to

$$s^{+}(\omega) = I^{+}(\omega) \quad \text{and} \quad s^{-}(\omega) = \lambda I^{-}(\omega). \tag{3}$$

This is done to correct for any difference in the intensity of the incoming and reflected laser beam and thus to assure that the area $A^{\pm} = \int s^{\pm}(\omega)\mathrm{d}\omega$ are identical. We consider $s^{+}(\omega), s^{-}(\omega)$ as different segments of $s(\omega)$, which cover both components of the profile. We then choose a frequency $\omega_\mathrm{s}$ close to the estimated frequency $\omega_0$ and minimize the quantity

$$\mathcal{S}(\omega_\mathrm{s}) = \sum_{i=1}^{N} |s(\omega_\mathrm{s} + i\Delta\omega) - s(\omega_\mathrm{s} - i\Delta\omega)|^2 \tag{4}$$

by variation of $\omega_\mathrm{s}$, where $\Delta\omega$ is a small interval, typically $1.7\times10^{-4}$ cm$^{-1}$ wide. The numbers $N$ must be sufficiently large, so that the interval $[\omega_\mathrm{s} - N\Delta\omega, \omega_\mathrm{s} + N\Delta\omega]$ covers both components of the line profile. The desired frequency $\omega_0$ is found, if

$$\mathcal{S}(\omega_0) = \min_{\omega_\mathrm{s}} \mathcal{S}(\omega_\mathrm{s}). \tag{5}$$

The numerical error of the procedure is estimated as follows. The error of the sum $\mathcal{S}(\omega_0)$ is calculated using the law of propagation of errors and uncertainties [29]. Afterwards, all frequencies $\omega_\mathrm{s}$ with a sum $\mathcal{S}(\omega_\mathrm{s})$ in the interval

$$I_\mathrm{error} = [\mathcal{S}(\omega_0) - \Delta\mathcal{S}(\omega_0), \mathcal{S}(\omega_0) + \Delta\mathcal{S}(\omega_0)] \tag{6}$$

are determined. The $\omega_\mathrm{s}$ with the largest deviation from $\omega_0$ yields the error of the resonance frequency:

$$\Delta\omega_0 = \max_{\omega_\mathrm{s}} |\omega_0 - \omega_s| \quad \forall\ \omega_\mathrm{s}\ \text{ with }\ \mathcal{S}(\omega_\mathrm{s}) \in I_\mathrm{error}. \tag{7}$$

The algorithm is insensitive to the choice of the starting value $\omega_\mathrm{s}$ as well as to the scaling parameter $\lambda$ for typical experimental conditions. Typical values of $\Delta\omega_0$ are in the range of 0.005 cm$^{-1}$. In measurements with low counting rates, resulting in a poor signal to noise ratio, the error rarely exceeds values of 0.01 cm$^{-1}$. Therefore, the line positions are determined with an accuracy of better than 0.01 cm$^{-1}$.

## 4 Determination of the molecular constants

### 4.1 Fit procedure

The $A^1\Sigma^+ \rightarrow X^1\Sigma^+$ LIF-spectra of NaH show only R- and P-lines. The combination differences $\Delta F''(J')$ between R- and P-lines of a vibrational band with the same rotational quantum number $J'$ are given by [30]:

$$\begin{aligned}\Delta F''(J') = {} & 4B_{v''}(J' + \frac{1}{2}) \\ & - D_{v''}[(J'+1)^2(J'+2)^2 - (J'-1)^2 J'^2] \\ & - H_{v''}[(J'+1)^3(J'+2)^3 - (J'-1)^3 J'^3].\end{aligned} \tag{8}$$

A least squares fit procedure, based on equation (8) and using the measured values $\Delta F''(J')$ yields the rotational constants $B_{v''}, D_{v''}$ and $H_{v''}$. A total of about 2800 transition frequencies are known. Here, we include only those 1000 transitions (including 283 from our experiment) for which the accuracy is known [5,6,8,12,14]. An iterative procedure is used to minimize the correlation between $B_{v''}$ and $D_{v''}$ or $H_{v''}$.

In a first step, the rotational constants $B_{v''}, D_{v''}$ and $H_{v''}$ are determined, using equation (8). The Dunham coefficients $Y_{k1}$ are then obtained by a fit procedure using:

$$B_{v''} = \sum_{k=0} Y_{k1} \left(v'' + \frac{1}{2}\right)^k. \tag{9}$$

The next step starts with the insertion of the constants $B^\mathrm{cal}_{v''}$ using the $Y_{k1}$ and equation (9) followed by another fit procedure to determine a modified value of $D_{v''}$.

Next, the Dunham coefficients $Y_{k2}$ are determined from a fit according to

$$D_{v''} = -\sum_{k=0} Y_{k2} \left(v'' + \frac{1}{2}\right)^k. \tag{10}$$

Finally, the constants $D^\mathrm{cal}_{v''}$ (using the $Y_{k2}$ from Eq. (10)) and $B^\mathrm{cal}_{v''}$ from equation (9) are inserted in equation (8) and the fit procedure is repeated to yield improved constants $H_{v''}$, based on which the Dunham coefficients $Y_{k3}$ are determined by a fit according to

$$H_{v''} = \sum_{k=0} Y_{k3} \left(v'' + \frac{1}{2}\right)^k. \tag{11}$$

The same procedure is applied for the determination of the Dunham coefficients for the $A$-state. Here, the differences of the termvalues $\Delta F'(J'')$ of R- and P-lines of a vibrational band with the same rotational quantum number $J''$ [30], obtained from the experiment, are used.

Finally, the band origins $\bar{\nu}_0(v'', v')$ are obtained from the differences of the transition frequencies between levels $(v', J')$ and $(v'', J'')$ and extrapolation to $J'' = 0$ [30]. The Dunham coefficients $Y_{k0}$ for the electronic ground state are obtained by a fit procedure based on

$$\Delta G(v'') = \sum_{k=1} Y_{k0} \left[\left(v'' + \frac{3}{2}\right)^k - \left(v'' + \frac{1}{2}\right)^k\right], \tag{12}$$

using the difference of transition frequencies $\Delta G(v'') = \bar{\nu}_0(v''+1, v') - \bar{\nu}_0(v'', v')$ for the band origins of the vibrational levels $v''$ and $v''+1$. An analogous procedure is used to derive the equivalent Dunham coefficients for the electronically excited state.

**Table 1.** Rotational constants in $cm^{-1}$ for the $X^1\Sigma^+$-state.

| $v''$ | $B_{v''}$ | $D_{v''}/\ 10^{-4}$ | $H_{v''}/\ 10^{-8}$ |
|---|---|---|---|
| 9 | 3.66340 ±0.00006 | 3.112 ±0.002 | 1.462 ±0.013 |
| 8 | 3.79275 ±0.00006 | 3.112 ±0.001 | 1.554 ±0.006 |
| 7 | 3.9214 ±0.0006 | 3.135 ±0.003 | 1.592 ±0.010 |
| 6 | 4.0486 ±0.0004 | 3.151 ±0.002 | 1.668 ±0.014 |
| 5 | 4.1777 ±0.0016 | 3.189 ±0.031 | 1.700 ±0.176 |
| 4 | 4.3050 ±0.0027 | 3.222 ±0.052 | 1.790 ±0.306 |
| 3 | 4.4365 ±0.0009 | 3.271 ±0.018 | 1.850 ±0.102 |
| 2 | 4.5670 ±0.0006 | 3.314 ±0.016 | 1.922 ±0.190 |
| 1 | 4.70002 ±0.00004 | 3.356 ±0.001 | 1.950 ±0.009 |
| 0 | 4.83502 ±0.00002 | 3.404 ±0.007 | 1.896 ±0.007 |

## 4.2 Rotational constants

The data of Lochbrunner *et al.* [12] show the least deviation between experimental data and calculated transition frequencies based on Dunham coefficients reported in the literature. Therefore, we compare our results to the data reported in reference [12] only.

### 4.2.1 Rotational constants of the $X^1\Sigma^+$ state

Our experimental data cover vibrational levels in the range $6 \leq v'' \leq 9$. The data base is extended to low vibrational levels by including the experimental results of Maki *et al.* [8] which cover the range $(0 \leq v'' \leq 2)$. Furthermore, Pankhurst [5] reports on combination differences for vibrational levels in the range $3 \leq v'' \leq 5$. The latter author do not offer an error analysis. Therefore, his data is not considered for the fit. However, his results are used to assess the quality of our new set of Dunham coefficients. We estimate the error of the transition frequencies calculated with their molecular constants to be of the order of 0.05 $cm^{-1}$. The new set of rotational constants is shown in Figure 4 and Table 1. Obviously, the data of Pankhurst are helpful to verify the quality of the new results.

The coefficients reported by Maki *et al.* for the $X^1\Sigma^+$ state, recommended by Stwalley *et al.* and used by Lochbrunner *et al.* are based on data restricted to the range $v'' \leq 3$. Therefore, it is not surprising, that these coefficients are not adequate for transitions involving higher vibrational levels. The deviation of their rotational constants $B_{v''}$ from our results is substantial for vibrational levels $v'' > 4$. Similarly, the new coefficients $D_{v''}$ and $H_{v''}$ are consistent with previously reported results for $v'' \leq 5$, but show substantial improvement for $v'' \geq 6$.

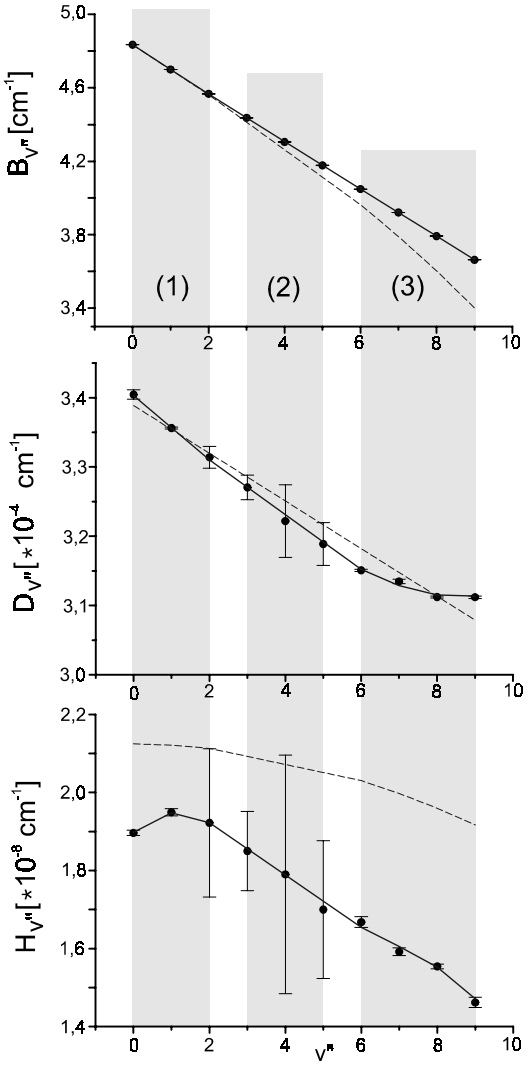


**Fig. 4.** Rotational constants of the $X^1\Sigma^+$-state of the NaH molecule, with the range of vibrational levels, experimentally covered by various authors indicated. (1) Maki *et al.* [8], (2) Pankhurst [5], (3) this work; full dots: experimental data; solid line: results from the analysis in this work; dashed line: results by Lochbrunner *et al.* [12].

### 4.2.2 Rotational constants of the $A^1\Sigma^+$ state

The fit procedure for the determination of the molecular constants for the first electronically excited state is based on our data which cover the range $2 \leq v' \leq 8$ and the experimental data by Orth *et al.* [6] $(v' = 0, 1)$, Lochbrunner [12] $(9 \leq v' \leq 15)$ and the molecule constants of Rafi *et al.* [14] $(16 \leq v' \leq 25)$. The new rotational constants as well as the data of Rafi *et al.* are indicated in Table 2 and Figure 5. The unusual shape of the potential energy curve of the $A^1\Sigma^+$-state is apparent from the vibrational level dependence of rotational constants $B_{v'}$ and $D_{v'}$, which show a pronounced maximum near $v' = 6$ and $v' = 3$, respectively.

The data of Lochbrunner *et al.* for $B_{v'}$ are not distinguishable from our results (and therefore not shown in Fig. 5). However, their results fail to adequately characterize the variation of $D_{v'}$ with $v'$. Our results confirm that Lochbrunner *et al.* justifiably neglected the constants $H_{v'}$ for the analysis of their data.

**Table 2.** Rotational constants in $cm^{-1}$ for the $A^1\Sigma^+$-state.

| $v'$ | $B_{v'}$ | $D_{v'}/10^{-4}$ | $H_{v'}/10^{-8}$ |
|---|---|---|---|
| 15 | 1.78338 ±0.00530 | 1.5222 ±0.0100 | –0.4000 ±0.0850 |
| 14 | 1.80424 ±0.00265 | 1.5139 ±0.0288 | –0.4000 ±0.0980 |
| 13 | 1.84068 ±0.00013 | 1.5253 ±0.0770 | –0.3500 ±0.0700 |
| 12 | 1.85680 ±0.00046 | 1.6100 ±0.0673 | –0.3300 ±0.0900 |
| 11 | 1.87792 ±0.00204 | 1.6205 ±0.0345 | –0.3260 ±0.0870 |
| 10 | 1.89332 ±0.00520 | 1.6509 ±0.0317 | 0.1512 ±0.1100 |
| 9 | 1.90560 ±0.00688 | 1.7070 ±0.0500 | 0.4083 ±0.2300 |
| 8 | 1.92374 ±0.00146 | 1.8257 ±0.0380 | 0.9480 ±0.2200 |
| 7 | 1.93847 ±0.00154 | 1.9200 ±0.0261 | 1.4610 ±0.1030 |
| 6 | 1.94166 ±0.00045 | 2.0340 ±0.0012 | 1.8405 ±0.0050 |
| 5 | 1.93987 ±0.00012 | 2.1308 ±0.0012 | 2.5148 ±0.0030 |
| 4 | 1.92901 ±0.00030 | 2.1982 ±0.0031 | 3.1539 ±0.0120 |
| 3 | 1.90981 ±0.00017 | 2.2696 ±0.0034 | 3.7330 ±0.0090 |
| 2 | 1.87321 ±0.00041 | 2.2598 ±0.0034 | 4.1390 ±0.0070 |
| 1 | 1.82186 ±0.00059 | 2.2014 ±0.0020 | 4.3285 ±0.0040 |
| 0 | 1.75080 ±0.00017 | 1.9720 ±0.0020 | 4.5135 ±0.0040 |

**Table 3.** Band origins ($v'$–$v''$).

| | band origin $\nu_0$ / $[cm^{-1}]$ | |
|---|---|---|
| band | this work | others |
| 9–8 | 16176.7 ±0.2 | - |
| 9–7 | 15817.2 ±0.1 | - |
| 9–6 | 15459.88 ±0.05 | - |
| 9–5 | 15105.86 ±0.05 | - |
| 8–6 | 16300.5 ±0.1 | 16300.5 [5] |
| 8–5 | 15946.4 ±0.1 | 15946.4 [5] |
| 8–4 | 15596.9 ±0.3 | - |
| 8–3 | 15253.1 ±0.3 | - |
| 7–5 | 16823.2 ±0.2 | 16823.4 [5] |
| 7–4 | 16473.8 ±0.1 | 16473.7 [5] |
| 7–3 | 16130.0 ±0.3 | 16130.1 [5] |
| 7–2 | 15792.8 ±0.4 | - |
| 6–4 | 17386.4 ±0.2 | 17386.6 [5] |
| 6–2 | 16705.5 ±0.4 | 16705.6 [5] |

**Table 4.** Variation of the vibrational level spacing $\Delta G(v'')$ with $v''$ for the $X^1\Sigma^+$-state.

| | $\Delta G(v'')/[cm^{-1}]$ | |
|---|---|---|
| $v''$ | this work | others |
| 8 | 840.4 ±0.2 | - |
| 7 | 876.5 ±0.3 | 876.9 ±0.1 [6] |
| 6 | 912.8 ±0.3 | 912.8 ±0.1 [6] |
| 5 | 948.2 ±0.6 | 948.8 [5] |
| 4 | 984.7 ±0.4 | 984.4 [5] |
| 3 | 1021.0 ±0.2 | 1021.0 [8] |
| 2 | 1057.8 ±0.2 | 1057.8 [8] |
| 1 | 1095.1 ±0.2 | 1095.1 [8] |
| 0 | 1133.2 ±0.2 | 1133.2 [8] |

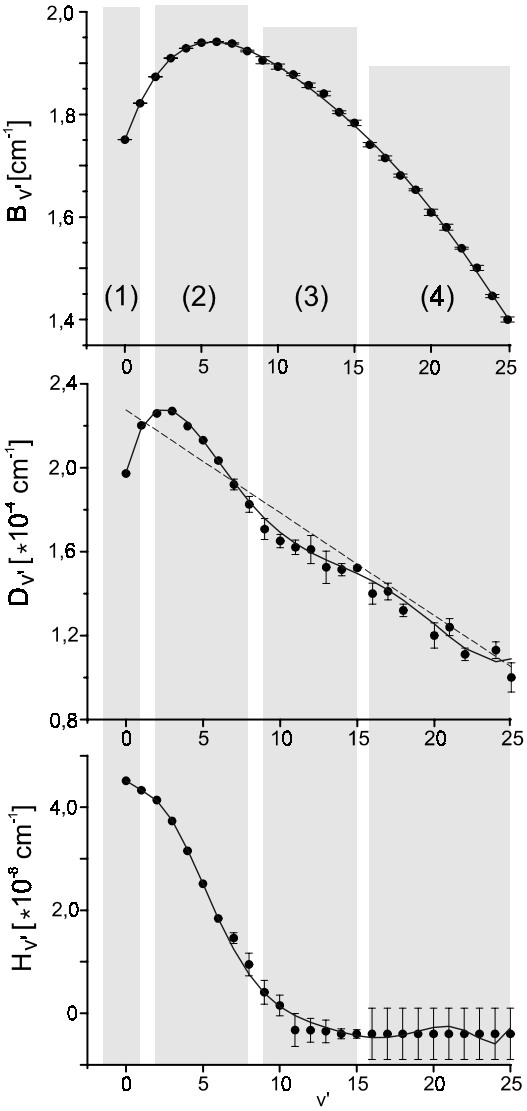


**Fig. 5.** Rotational constants of the $A^1\Sigma^+$-state of the NaH-molecule, with the range of vibrational levels, experimentally covered by various authors indicated. (1) Orth *et al.* [6], (2) this work, (3) Lochbrunner *et al.* [12], (4) Rafi *et al.* [14]; full dots: experimental data; solid line: results from the analysis in this work; dashed line: results by Lochbrunner *et al.* [12].

### 4.3 Vibrational constants

The determination of the vibrational constants is based on our data for the band origins (Tab. 3) and data of Maki *et al.* [8], Orth *et al.* [6] and Lochbrunner *et al.* [12]. Excellent agreement with the previously published data for the band origins and vibrational level spacings (Tabs. 3, 4 and 5 as well as Fig. 6) is found up to level $v'' = 8$ and $v' \approx 25$, respectively.

### 4.4 Dunham coefficients

The new set of Dunham coefficients of the $X^1\Sigma^+$-state and the $A^1\Sigma^+$-state is listed in Table 6. The electronic

**Table 5.** Variation of the vibrational level spacing $\Delta G(v')$ with $v'$ for the $A^1\Sigma^+$-state.

| | $\Delta G(v')/[\mathrm{cm}^{-1}]$ | |
|---|---|---|
| $v'$ | this work | others |
| 14 | 348.7 ±0.5 | 348.5 ±0.8 [12] |
| 13 | 352.0 ±0.7 | 351.8 ±0.7 [12] |
| 12 | 354.9 ±0.7 | 354.9 ±0.7 [12] |
| 11 | 357.8 ±0.7 | 357.8 ±0.7 [12] |
| 10 | 359.3 ±0.6 | 359.3 ±0.6 [12] |
| 9 | 360.2 ±0.6 | 360.2 ±0.6 [12] |
| 8 | 360.7 ±0.8 | 360.7 ±0.6 [12] |
| 7 | 359.0 ±0.3 | 359.2 [5] |
| 6 | 357.2 ±0.2 | 357.5 ±0.7 [12] |
| 5 | 354.0 ±0.1 | 353.9 ±0.6 [12] |
| 4 | 349.7 ±0.4 | 349.7 ±0.7 [12] |
| 3 | 343.6 ±0.4 | 343.6 ±0.7 [12] |
| 2 | 337.2 ±0.7 | 337.2 ±0.7 [12] |
| 1 | 329.9 ±0.2 | 329.9 [5] |
| 0 | 323.76 ±0.2 | 323.84 [6] |

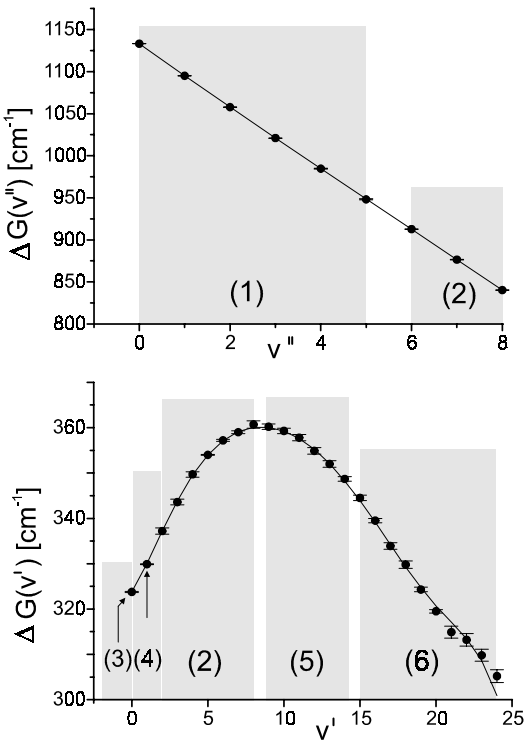


**Fig. 6.** The variation of vibrational level spacing $\Delta G$ for the $X^1\Sigma^+$- and $A^1\Sigma^+$-state of NaH. (1) Maki *et al.* [8], (2) this work, (3) Orth *et al.* [6], (4) Pankhurst *et al.* [5], (5) Lochbrunner *et al.* [12], (6) Rafi *et al.* [14]. Full dots: experimental data; solid line: results from the analysis in this work.

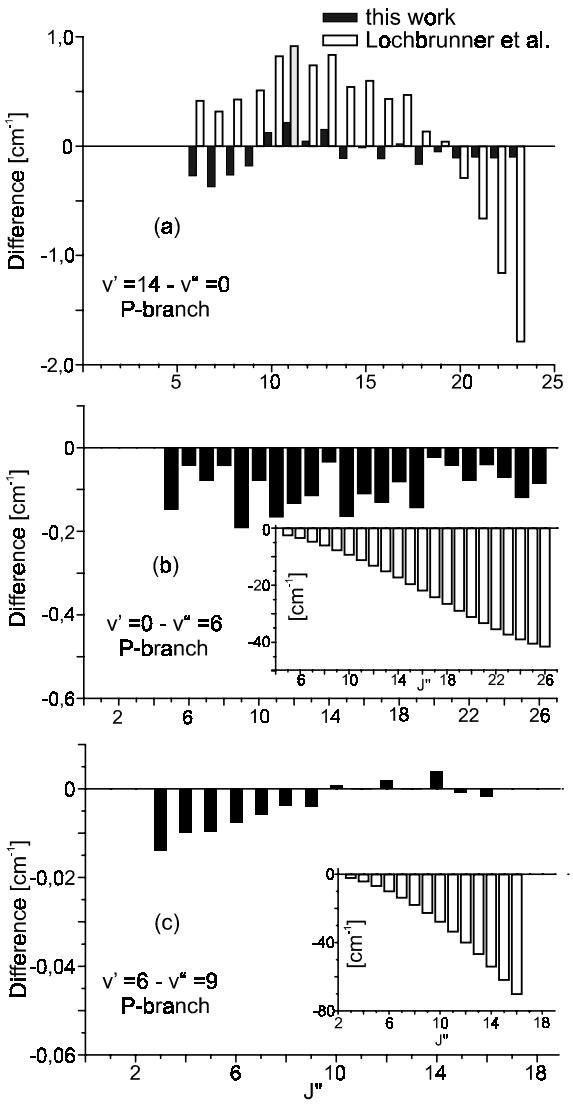


**Fig. 7.** Deviation of calculated term values from the measured ones, using the Dunham coefficients from this work and from Lochbrunner *et al.* [12].

excitation energy $T_{\mathrm{el}}$ is required for the calculation of the transition frequencies. According to Stwalley *et al.* [11] this energy difference is $T_{\mathrm{el}} = 22\,713 \pm 5\ \mathrm{cm}^{-1}$. With $T_{\mathrm{el}} = 22\,713.0\ \mathrm{cm}^{-1}$ we find a constant deviation of 0.2 $\mathrm{cm}^{-1}$ of the measured and calculated transition frequencies. Excellent agreement is found for $T_{\mathrm{el}} = 22\,713.2\ \mathrm{cm}^{-1}$.

The quality of the new Dunham coefficients is demonstrated by inspection of the deviation of a representative set of measured term value differences from those calculated. Figure 7a shows the deviation of calculated and measured values for the 0–14 band, based on experimental data from reference [12]. The latter are determined with an accuracy of the line positions of 0.2 $\mathrm{cm}^{-1}$. Based on our new coefficients, the rms deviation of measured and calculated term value is $\leq 0.1\ \mathrm{cm}^{-1}$ for the data shown in Figure 7a, with a maximum deviation of 0.4 $\mathrm{cm}^{-1}$. The experimental data reported by Orth *et al.* [6], see Fig. 7b),

**Table 6.** Dunham coefficients in $cm^{-1}$ for NaH.

| coefficient | Lochbrunner *et al.* [8] | this work | Lochbrunner *et al.* [12] | this work |
|---|---|---|---|---|
| | $X^1\Sigma^+$ | | $A^1\Sigma^+$ | |
| $T_{el}$ | | | 22713 ± 5 | 22713.2 |
| $Y_{00}$ | 0.59 | 0.55 | 0.86 | 0.45 |
| $Y_{10}$ | 1171.75909 | 1171.968±0.012 | 317.56 | 319.96±0.08 |
| $Y_{20}$ | −19.52352 | −19.703 ± 0.010 | 2.701 | 0.7783±0.083 |
| $Y_{30}$ | 0.12131 | 0.175±0.002 | 0.02731 | 0.908±0.031 |
| $Y_{40} \times 10^3$ | −0.59 | −6.58 ± 0.15 | −43.29 | −147.2 ± 5.5 |
| $Y_{50} \times 10^4$ | −2.235 | | 21.59 | 114±5.5 |
| $Y_{60} \times 10^5$ | | | −5.25 | −50.7 ± 3.0 |
| $Y_{70} \times 10^7$ | | | 5.3 | 121.7±8.5 |
| $Y_{80} \times 10^7$ | | | | −1.207 ± 0.97 |
| $Y_{01}$ | 4.90336382 | 4.90327±0.00013 | 1.7121 | 1.70553±0.00056 |
| $Y_{11}$ | −0.13709097 | −0.137 ± 0.00036 | 0.09152 | 0.0971±0.0008 |
| $Y_{21} \times 10^3$ | 1.111351 | 1.01±0.23 | −12.09 | −13.7 ± 0.3 |
| $Y_{31} \times 10^4$ | −0.3492 | −0.007443 ± 0.4 | 6.50 | 8.21±0.4 |
| $Y_{41} \times 10^5$ | | −0.355 ± 0.2 | −1.80 | −2.55 ± 0.21 |
| $Y_{51} \times 10^7$ | | | 1.9 | 3.06±0.39 |
| $Y_{02} \times 10^4$ | −3.434285 | −3.425 ± 0.013 | −2.30 | −1.808 ± 0.016 |
| $Y_{12} \times 10^6$ | 4.9065 | 4.4±1.2 | 4.9 | −38.6 ± 2.6 |
| $Y_{22} \times 10^8$ | −9.025 | 15.77±2.4 | | 1020±120 |
| $Y_{32} \times 10^8$ | | −2.9 ± 1.4 | | −100 ± 22 |
| $Y_{42} \times 10^8$ | | | | 4.68±1.9 |
| $Y_{52} \times 10^9$ | | | | −1.013 ± 0.75 |
| $Y_{62} \times 10^{12}$ | | | | 7.78±11 |
| $Y_{03} \times 10^8$ | 2.1246 | 1.83±0.026 | | 4.727±0.019 |
| $Y_{13} \times 10^{11}$ | 1.641 | 171±48 | | −593 ± 50 |
| $Y_{23} \times 10^{11}$ | −2.476 | −75 ± 22 | | 403±41 |
| $Y_{33} \times 10^{10}$ | | 0.96±0.4 | | −15.6 ± 1.5 |
| $Y_{43} \times 10^{12}$ | | −4.23 ± 1.88 | | 252±27 |
| $Y_{53} \times 10^{11}$ | | | | −2.1 ± 0.3 |
| $Y_{63} \times 10^{13}$ | | | | 9.56±1.4 |
| $Y_{73} \times 10^{14}$ | | | | −2.26 ± 0.4 |
| $Y_{83} \times 10^{16}$ | | | | 2.1715±0.461 |

are reproduced with a rms deviation for the data shown of $\leq 0.1$ $cm^{-1}$ and a maximum deviation of 0.2 $cm^{-1}$. Finally, the experimental data from our work are reproduced with a rms deviation of $\leq 0.01$ $cm^{-1}$ and a maximum difference of 0.02 $cm^{-1}$. The deviation of the measured and calculated term value difference, based on the coefficients reported in [12] (see Figs. 7a and the inset in Figs. 7b and 7c), is significantly larger.

## 5 Potential energy curves

The turning points of the RKR potential [31–33] for the $X^1\Sigma^+$ and $A^1\Sigma^+$ states of NaH were calculated using a computer program reported by Tellinghuisen [34]. The input parameters are the rotational constants $B_v$ and the vibrational part of the termvalues, $G(v) + Y_{00}$, where $Y_{00}$ is the Dunham correction [1]:

$$Y_{00} = \frac{Y_{01}}{4} - \frac{Y_{11}Y_{10}}{12Y_{01}} + \frac{Y_{11}^2 Y_{10}^2}{144Y_{01}^3} + \frac{Y_{20}}{4} \cdot \qquad (13)$$

The results based on the new rotational and vibrational constants for the $X^1\Sigma^+$ and $A^1\Sigma^+$ states are given in Tables 7 and 8, respectively.

## 6 Summary

We have demonstrated a novel laser spectroscopic sub-Doppler method, based on crossed beams reactive scattering and capable of sub-Doppler resolution. Accurate determination of the transition frequencies is possible, when the Doppler shift $|\mathbf{k} \cdot \mathbf{V}_s|$ relative to the resonance

**Table 7.** Classical turning points of the RKR-potential of the $X^1\Sigma^+$-state.

| $v''$ | $G(v'')/$ cm$^{-1}$ | $R_-$/Å | $R_+$/Å |
|---|---|---|---|
| 0 | 581.63 ±0.1 | 1.7284 ±0.0001 | 2.0794 ±0.0001 |
| 1 | 1714.73 ±0.1 | 1.6336 ±0.0001 | 2.2417 ±0.0001 |
| 2 | 2809.80 ±0.1 | 1.5741 ±0.0005 | 2.3708 ±0.0005 |
| 3 | 3867.59 ±0.1 | 1.5298 ±0.0011 | 2.4866 ±0.0011 |
| 4 | 4888.67 ±0.1 | 1.4943 ±0.0008 | 2.5956 ±0.0008 |
| 5 | 5873.45 ±0.1 | 1.4646 ±0.0005 | 2.7009 ±0.0005 |
| 6 | 6822.20 ±0.1 | 1.4392 ±0.0005 | 2.8041 ±0.0005 |
| 7 | 7735.02 ±0.1 | 1.4170 ±0.0006 | 2.9067 ±0.0006 |
| 8 | 8611.86 ±0.1 | 1.3975 ±0.0005 | 3.0097 ±0.0005 |
| 9 | 9452.50 ±0.1 | 1.3799 ±0.0004 | 3.1142 ±0.0004 |

**Table 8.** Classical turning points of the RKR-potential of the $A^1\Sigma^+$-state.

| $v'$ | $G(v')$/cm$^{-1}$ | $R_-$/Å | $R_+$/Å |
|---|---|---|---|
| 0 | 160.73 ±0.3 | 2.8573 ±0.0001 | 3.5141 ±0.0002 |
| 1 | 484.54 ±0.3 | 2.608 ±0.001 | 3.746 ±0.001 |
| 2 | 814.65 ±0.3 | 2.448 ±0.002 | 3.905 ±0.002 |
| 3 | 1151.82 ±0.3 | 2.330 ±0.002 | 4.038 ±0.002 |
| 4 | 1495.67 ±0.3 | 2.237 ±0.002 | 4.157 ±0.002 |
| 5 | 1845.23 ±0.3 | 2.161 ±0.001 | 4.268 ±0.001 |
| 6 | 2199.26 ±0.3 | 2.098 ±0.001 | 4.375 ±0.001 |
| 7 | 2556.50 ±0.3 | 2.044 ±0.002 | 4.479 ±0.002 |
| 8 | 2915.76 ±0.3 | 1.997 ±0.002 | 4.581 ±0.002 |
| 9 | 3275.96 ±0.3 | 1.956 ±0.006 | 4.682 ±0.006 |
| 10 | 3636.14 ±0.3 | 1.919 ±0.009 | 4.782 ±0.009 |
| 11 | 3995.44 ±0.3 | 1.886 ±0.010 | 4.882 ±0.010 |
| 12 | 4353.04 ±0.3 | 1.857 ±0.010 | 4.983 ±0.010 |
| 13 | 4708.19 ±0.3 | 1.829 ±0.010 | 5.084 ±0.010 |
| 14 | 5060.16 ±0.3 | 1.804 ±0.010 | 5.185 ±0.010 |
| 15 | 5408.32 ±0.3 | 1.781 ±0.010 | 5.288 ±0.010 |
| 16 | 5752 ±1.1 | 1.760 ±0.009 | 5.392 ±0.009 |
| 17 | 6091 ±1.8 | 1.740 ±0.008 | 5.498 ±0.008 |
| 18 | 6425 ±2.6 | 1.722 ±0.006 | 5.606 ±0.006 |
| 19 | 6754 ±3.1 | 1.706 ±0.006 | 5.714 ±0.006 |
| 20 | 7079 ±3.5 | 1.691 ±0.006 | 5.823 ±0.006 |
| 21 | 7399 ±4.8 | 1.679 ±0.007 | 5.933 ±0.007 |
| 22 | 7715 ±6.2 | 1.668 ±0.006 | 6.042 ±0.006 |
| 23 | 8027 ±7.5 | 1.660 ±0.006 | 6.153 ±0.006 |
| 24 | 8335 ±8.9 | 1.653 ±0.006 | 6.265 ±0.006 |
| 25 | 8636 ±10.3 | 1.646 ±0.006 | 6.384 ±0.006 |

frequency is sufficiently large to allow the spectral resolution of the profiles induced by counterpropagating laser beams.

We have presented new spectroscopic data for the $A$–$X$ transition with an experimental accuracy of the individual transition frequencies of better than 0.01 cm$^{-1}$, involving relatively high vibrational levels $6 \le v'' \le 9$ in the electronic ground state. New Dunham coefficients were derived based on our data and on previously published ones. They predict the known line positions to better than 0.1 cm$^{-1}$ (rms value) with a maximum deviation of 0.4 cm$^{-1}$ for the vibrational levels $0 \le v'' \le 9$ of the $X^1\Sigma^+$ state and $0 \le v' \le 25$ of the $A^1\Sigma^+$ state.

We have identified the cause for the sometimes large deviation between the measured and calculated line positions (known from previous work): the previously available accuracy of the rotational constants $B_{v''}$ (for $v'' > 2$) and $D_{v'}$ (in the range where it exhibit a maximum) was inadequate. This deficiency is overcome with our work.

We thank W. Meyer, P. Dern, S. Lochbrunner, H. Theuer, S. Scherer and P. Dittmann for valuable discussions. This work was supported by the Deutsche Forschungsgemeinschaft. Partial support was also received through the European Union under HCM ERB-CHR-XCT-94-0603.

## Appendix A: Wavenumbers of the measured line positions

| $J''$ | band: $v''$=6–$v'$=2 | | band: $v''$=6–$v'$=4 | |
|---|---|---|---|---|
| | R-branch [cm$^{-1}$] | P-branch [cm$^{-1}$] | R-branch [cm$^{-1}$] | P-branch [cm$^{-1}$] |
| 21 | 15796.213 | 15650.829 | | |
| 22 | 15707.757 | 15556.905 | | |
| 23 | 15615.599 | 15459.430 | | |
| 24 | 15519.840 | 15358.489 | | |
| 25 | 15420.572 | 15254.163 | | |
| 26 | 15317.870 | 15146.545 | | 15863.279 |
| 27 | 15211.864 | 15035.743 | | 15755.036 |
| 28 | 15102.642 | | 15829.490 | 15643.719 |
| 29 | | | | 15529.437 |
| 30 | | | | |
| 31 | 14756.834 | | | |

| $J''$ | band: $v''$=7–$v'$=2 | | band: $v''$=7–$v'$=3 | |
|---|---|---|---|---|
| | R-branch [cm$^{-1}$] | P-branch [cm$^{-1}$] | R-branch [cm$^{-1}$] | P-branch [cm$^{-1}$] |
| 11 | 15567.762 | 15484.221 | | |
| 12 | 15522.632 | 15432.323 | | |
| 13 | 15473.506 | 15376.574 | | 15719.076 |
| 14 | 15420.447 | 15316.990 | 15765.857 | 15660.396 |
| 15 | 15363.474 | 15253.625 | 15709.980 | 15597.998 |
| 16 | 15302.631 | 15186.522 | 15650.290 | 15531.936 |
| 17 | 15237.966 | 15115.726 | | 15462.231 |
| 18 | 15169.519 | 15041.287 | 15519.668 | 15388.952 |
| 19 | 15097.362 | 14963.267 | 15448.817 | 15312.146 |
| 20 | 15021.539 | 14881.727 | 15374.358 | 15231.871 |
| 21 | | | 15296.343 | 15148.190 |
| 22 | | | 15214.840 | 15061.168 |
| 23 | | | 15129.922 | 14970.876 |
| 24 | | | 15041.287 | |

| $J''$ | band: $v''$=7–$v'$=4 | | band: $v''$=7–$v'$=5 | |
|---|---|---|---|---|
| | R-branch [cm$^{-1}$] | P-branch [cm$^{-1}$] | R-branch [cm$^{-1}$] | P-branch [cm$^{-1}$] |
| 13 | | 16066.234 | | |
| 14 | 16114.901 | 16008.134 | | |
| 15 | 16059.756 | 15946.366 | | |
| 16 | 16000.840 | 15880.972 | | |
| 17 | 15938.211 | 15812.004 | | |
| 18 | 15871.896 | 15739.495 | | |
| 19 | | 15663.511 | | |
| 20 | 15728.439 | 15584.100 | 16083.750 | 15938.277 |
| 21 | 15651.401 | 15501.324 | 16007.318 | 15856.055 |
| 22 | 15570.905 | 15415.248 | 15927.465 | 15770.559 |
| 23 | 15487.031 | 15325.939 | 15844.243 | 15681.855 |
| 24 | 15399.837 | 15233.469 | 15757.723 | 15590.015 |
| 25 | 15309.404 | 15137.915 | 15667.987 | 15495.123 |
| 26 | 15215.822 | 15039.363 | 15575.108 | 15397.251 |
| 27 | | | 15479.175 | 15296.476 |

| $J''$ | band: $v''$=8–$v'$=3 | | band: $v''$=8–$v'$=4 | |
|---|---|---|---|---|
| | R-branch [cm$^{-1}$] | P-branch [cm$^{-1}$] | R-branch [cm$^{-1}$] | P-branch [cm$^{-1}$] |
| 2 | 15253.293 | 15234.225 | | |
| 3 | 15245.785 | 15219.133 | | |
| 4 | 15234.509 | 15200.307 | | |
| 5 | 15219.457 | 15177.754 | | |
| 6 | 15200.634 | 15151.491 | | |
| 7 | 15178.055 | 15121.538 | 15523.386 | 15466.233 |
| 8 | 15151.725 | | 15497.439 | 15432.901 |
| 9 | 15121.662 | 15050.612 | 15467.805 | 15395.970 |
| 10 | | 15009.704 | 15434.498 | 15355.457 |
| 11 | 15050.382 | 14965.244 | 15050.382 | 14965.244 |
| 12 | | | 15356.949 | 15263.808 |
| 13 | | | 15312.751 | 15212.736 |
| 14 | | | 15264.973 | 15158.212 |
| 15 | | | 15213.656 | 15100.274 |
| 16 | | | 15158.829 | 15038.964 |
| 17 | | | 15100.531 | 14974.327 |
| 18 | | | 15038.815 | 14906.413 |
| 19 | | | 14973.717 | 14835.272 |
| 20 | | | 14905.299 | 14760.958 |
| 21 | | | 14833.612 | 14683.535 |

| $J''$ | band: $v''$=8–$v'$=5 | | band: $v''$=8–$v'$=6 | |
|---|---|---|---|---|
| | R-branch [cm$^{-1}$] | P-branch [cm$^{-1}$] | R-branch [cm$^{-1}$] | P-branch [cm$^{-1}$] |
| 13 | | | 16019.413 | 15918.491 |
| 14 | 15617.288 | 15509.757 | 15972.167 | 15864.395 |
| 15 | 15566.385 | 15452.208 | 15921.425 | 15806.933 |
| 16 | 15512.008 | 15391.276 | 15867.231 | 15746.145 |
| 17 | 15454.196 | 15327.055 | 15809.623 | 15682.095 |
| 18 | 15392.991 | 15259.592 | 15748.649 | 15614.816 |
| 19 | 15328.447 | 15188.936 | 15684.347 | 15544.365 |
| 20 | | 15115.139 | 15616.774 | 15470.795 |
| 21 | 15189.529 | 15038.265 | 15545.990 | 15394.169 |
| 22 | | | 15472.048 | 15314.551 |
| 23 | | | 15395.016 | |

| $J''$ | band: $v''$=9–$v'$=5 | | band: $v''$=9–$v'$=6 | |
|---|---|---|---|---|
| | R-branch [cm$^{-1}$] | P-branch [cm$^{-1}$] | R-branch [cm$^{-1}$] | P-branch [cm$^{-1}$] |
| 1 | 15110.233 | 15098.599 | 15464.265 | |
| 2 | 15107.204 | | | |
| 3 | 15100.712 | 15073.640 | 15454.783 | 15427.673 |
| 4 | 15090.784 | 15056.026 | 15444.868 | 15410.076 |
| 5 | 15077.400 | 15035.013 | 15431.518 | 15389.077 |
| 6 | 15060.574 | 15010.612 | 15414.724 | 15364.699 |
| 7 | 15040.319 | 14982.845 | 15394.518 | 15336.961 |
| 8 | 15016.643 | 14951.733 | 15370.899 | 15305.886 |
| 9 | 14989.568 | 14917.311 | 15343.888 | 15271.498 |
| 10 | 14959.102 | 14879.574 | 15313.503 | 15233.831 |
| 11 | 14925.275 | 14838.584 | 15279.770 | 15192.905 |
| 12 | 14888.107 | 14794.360 | 15242.713 | 15148.763 |
| 13 | 14847.621 | 14746.940 | 15202.354 | 15101.434 |
| 14 | | | 15158.732 | 15050.965 |
| 15 | | | 15111.878 | 14997.385 |
| 16 | | | 15061.827 | 14940.748 |

| $J''$ | band: $v''$=9–$v'$=7 | | band: $v''$=9–$v'$=8 | |
|---|---|---|---|---|
| | R-branch [cm$^{-1}$] | P-branch [cm$^{-1}$] | R-branch [cm$^{-1}$] | P-branch [cm$^{-1}$] |
| 4 | | 15767.266 | | |
| 5 | 15788.603 | 15746.158 | | |
| 6 | 15771.764 | 15721.820 | | |
| 7 | 15751.501 | 15694.048 | | |
| 8 | 15727.822 | 15662.921 | | |
| 9 | 15700.751 | 15628.480 | | |
| 10 | 15670.307 | 15590.753 | | |
| 11 | 15636.515 | 15549.771 | 15994.520 | 15908.127 |
| 12 | 15599.402 | 15505.566 | 15957.212 | 15863.751 |
| 13 | 15558.993 | 15458.179 | 15916.608 | 15816.185 |
| 14 | 15515.320 | 15407.650 | 15872.734 | 15765.464 |
| 15 | 15468.426 | 15354.022 | 15825.630 | 15711.640 |
| 16 | 15418.344 | 15297.337 | 15775.340 | |

## References


1. J.L. Dunham, Phys. Rev. **41**, 713 (1932).
2. T. Hori, Z. Phys. **62**, 353 (1930).
3. T. Hori, Z. Phys. **71**, 478 (1931).
4. E. Olsson, Z. Phys. **93**, 206 (1935).
5. R.C. Pankhurst, Proc. Phys. Soc. Lond. A **62**, 191 (1949).
6. F.B. Orth, W.C. Stwalley, S.C. Yang, Y.K. Hsieh, J. Mol. Spec. **79**, 314 (1980).
7. K.V.L.N. Sastry, E. Herbst, F.C. DeLucia, J. Chem. Phys. **75**, 4753 (1981).
8. A.G. Maki, W.B. Olson, J. Chem. Phys. **90**, 6887 (1989).
9. K.R. Leopold, L.R. Zink, K.M. Evenson, D.A. Jennings, J. Mol. Spectrosc. **122**, 150 (1987).
10. U. Magg, H. Jones, Chem. Phys. Lett. **146**, 415 (1988).
11. W.C. Stwalley, W.T. Zemke, S.C. Yang, J. Chem. Phys. Ref. Data **20**, 153 (1991).
12. S. Lochbrunner, M. Motzkus, G. Pichler, K.L. Kompa, P. Hering, Z. Phys. D **38**, 35 (1996).
13. R. Al-Tuwirqi, A. Bakry, M. Rafi, Fayyazuddin, J. Phys. B: At. Mol. Opt. Phys. **30**, 2033 (1997).
14. M. Rafi, N. Ali, K. Ahmad, I.A. Khan, M.A. Baig, Z. Iqbal, J. Phys. B: At. Mol. Opt. Phys. **26**, L129 (1993).

15. M. Giroud, O. Nedelec, J. Chem. Phys. **73**, 4151 (1980).
16. O. Nedelec, M. Giroud, J. Chem. Phys. **79**, 2121 (1983).
17. O. Nedelec, M. Giroud, J. Chem. Phys. **80**, 2987 (1984).
18. J.T. Bahns, C.C. Tsai, B. Ji, J.T. Kim, G. Zhao, W.C. Stwalley, J.C. Block, R.W. Field, J. Mol. Phys. **186**, 222 (1997).
19. E.S. Sachs, J. Hinze, N.H. Sabelli, J. Chem. Phys. **62**, 3367 (1975).
20. E.S. Sachs, J. Hinze, N.H. Sabelli, J. Chem. Phys. **62**, 3377 (1975).
21. E.S. Sachs, J. Hinze, N.H. Sabelli, J. Chem. Phys. **62**, 3384 (1975).
22. H.H. Telle, J. Mol. Struc. **143**, 565 (1986).
23. A. Pardo, J.J. Camacho, J.M.L. Poyato, E. Martin, Chem. Phys. **121**, 41 (1988).
24. F.P. Pesl, P. Dern, K. Bergmann (to be published, 1999).
25. K. Bergmann, U. Hefter, P. Hering, Chem. Phys. **32**, 329 (1978).
26. U. Hefter, K. Bergmann, in *Atomic and molecular beam methods*, edited by G. Scoles (Oxford University Press, 1988).
27. S. Gerstenkorn, P. Luc, *Atlas du Spectre d'absorption de la molécule d'iode* (Éditions du CNRS, 1978).
28. H. Dörr, P. Dern, W. Meyer (1999, personal communication).
29. W.H.H. Gränicher, *Messung beendet- was nun?*, Hochschulverlag AG an der ETH Zürich, B.G. Teubner Stuttgart, 1996.
30. G. Herzberg, *Spectra of diatomic molecules* (van Nostrand Reinhold, New York, 1950).
31. R. Rydberg, Graphische Darstellung einiger bandenspektroskopischer Ergebnisse, Z. Phys. **73**, 376 (1931).
32. O. Klein, Z. Phys. **76**, 226 (1932).
33. A. Rees, Proc. Phys. Soc. **59**, 998 (1947).
34. J. Tellinghuisen, Comp. Phys. Commun. **6**, 221 (1974).